

Solar wind speed within 20 R_S of the Sun estimated from limb coronal mass ejections

Tomoko Nakagawa,¹ Nat Gopalswamy,² and Seiji Yashiro^{3,4}

Received 30 May 2005; revised 16 September 2005; accepted 18 November 2005; published 27 January 2006.

[1] An estimation of the solar wind speed in the vicinity of the Sun is carried out using the initial speed and acceleration of coronal mass ejections (CMEs) that appeared close to the solar limb. A linear relationship was found between the initial acceleration and the speed of the limb CMEs. It appears that a dragging force is acting on the CMEs, depending on the speed difference between the CMEs and the ambient plasma. The ambient solar wind speed within 20 solar radii estimated from low-latitude CMEs during 1998–2003 ranged from 100 to 700 km s^{−1}, while the solar wind speed measured at 1 AU ranged from 300 to 700 km s^{−1}. The estimated solar wind speeds in the vicinity of the Sun sometimes agreed with the simultaneous in situ measurements at 1 AU, but in other periods they were slower than the speeds measured at 1 AU. It is suggested that most of the time the low-latitude solar wind completes accelerating within 20 solar radii, but occasionally additional acceleration is present beyond 20 solar radii.

Citation: Nakagawa, T., N. Gopalswamy, and S. Yashiro (2006), Solar wind speed within 20 R_S of the Sun estimated from limb coronal mass ejections, *J. Geophys. Res.*, *111*, A01108, doi:10.1029/2005JA011249.

1. Introduction

[2] Observational information on the solar wind velocity in the very site of acceleration is essential to understand the acceleration mechanism, but there has been no in situ measurement in the vicinity of the Sun. At present, it is still difficult to send a spacecraft to the Sun. Remote sensing techniques have been employed to observe mass motion near the Sun (white light, H α , radio, and interplanetary scintillation observations). Among them, successive white light images have enabled us to track coronal mass ejections (CMEs). Although the speed of CMEs may be different from the speed of ambient solar wind, they provide us a unique opportunity to get information on initial speeds of the solar wind material just after the ejection from the Sun.

[3] Table 1 lists the literature in which speeds of CMEs were compared with those of the interplanetary counterparts. Gosling *et al.* [1975] compared a Skylab CME with a large interplanetary shock detected by Pioneer 9. The speed of the CME, 960 km s^{−1}, was close to the transit speed, 950 km s^{−1}, calculated from the time difference, while the local shock speed was 720 km s^{−1}, suggesting that the CME decelerated in interplanetary space. For an interplanetary magnetic cloud (MC) detected by Helios 1 associated with a P78-1/Solwind CME [Burlaga *et al.*, 1982], the local MC

speed (470 ± 10 km s^{−1}) was close to the CME transit speed (500 km s^{−1}). On the basis of P78-1/Solwind coronagraphs and Helios 1 and 2 observations, Schwenn [1983] showed that the speeds of flare-related CMEs agreed with the mean transit speeds as well as the local shock speeds in interplanetary space, while other CMEs had postacceleration or deceleration. Sheeley *et al.* [1985] analyzed a set of shocks associated with fast CMEs (>500 km s^{−1}) and found that the local speeds were smaller than the average transit speeds, indicating deceleration. Lindsay *et al.* [1999] found that slow CMEs are accelerated in interplanetary space, while fast CMEs are decelerated [e.g., Lindsay *et al.*, 1999, Figure 5]. All these papers clearly indicate that the ambient medium affects CME propagation. Gopalswamy *et al.* [2000, 2001a] quantified this coupling in the form of interplanetary acceleration. We adopt the same method to estimate the speed of the ambient plasma within the coronagraph field of view.

[4] On the basis of SOHO/LASCO and WIND observations, Gopalswamy *et al.* [2000] presented a linear relationship between the initial speeds of CMEs and their average accelerations during their passage from the Sun to spacecraft at 0.8–1.0 AU. To minimize projection effects, Gopalswamy *et al.* [2001a] used limb CMEs and data from spacecraft in quadrature and obtained the empirical relation

$$a = c_0 + c_1 u_0, \quad (1)$$

where u_0 is the initial speed of CMEs and a is the effective acceleration during their travel from the Sun to 1 AU. The linear relationship, rewritten as

$$a = c_1(u_0 - u_c), \quad (2)$$

¹Information and Communication Engineering, Tohoku Institute of Technology, Sendai, Japan.

²NASA Goddard Space Flight Center, Greenbelt, Maryland, USA.

³Catholic University of America, Washington, D. C., USA.

⁴Also at NASA Goddard Space Flight Center, Greenbelt, Maryland, USA.

Table 1. Studies Relating Coronal Mass Ejections in Coronagraphs to Their Interplanetary Counterparts

Literature	Coronagraph	Interplanetary Measurement	Period
<i>Gosling et al.</i> [1975]	Skylab/HAO	Pioneer 9	1973
<i>Burlaga et al.</i> [1982]	P78-1/Solwind	Helios 1	1980
<i>Schwenn</i> [1983]	P78-1/Solwind	Helios 1,2	1979–1981
<i>Sheeley et al.</i> [1985]	P78-1/Solwind	Helios1	1979–1982
<i>Richardson et al.</i> [1994]	SMM coronagraph	ICE,IMP8	1989
<i>Lindsay et al.</i> [1999]	Solwind, SMM	Helios	1979–1982
		PVO	1979–1988
<i>Gopalswamy et al.</i> [2000]	SOHO/LASCO	WIND	1996–1998
<i>Gopalswamy et al.</i> [2001a]	Solwind	Helios	1979–1982
		PVO	1979–1988

suggests that the CMEs are accelerated or decelerated depending on their difference in speed from a certain critical speed

$$u_c = -c_0/c_1. \quad (3)$$

The critical speed $u_c = 406 \text{ km s}^{-1}$ calculated from the empirical parameters $c_0 = 2.193$ and $c_1 = -0.0054$ is remarkably close to the asymptotic solar wind speed in the equatorial plane [*Gopalswamy et al.*, 2001a]. The negative sign of c_1 indicates that the fast CMEs are decelerated while the slow CMEs are accelerated.

[5] It seems likely that the critical speed u_c gives some measure of the speed of the ambient plasma surrounding CMEs. If a similar relationship

$$a_0 = c_1(u_0 - u_c) \quad (4)$$

holds between the initial speed u_0 and the initial acceleration a_0 of CMEs within 20 solar radii from the Sun, we will be able to estimate the speed of the “ambient” solar wind in the vicinity of the Sun. Indeed, Figure 8 of *Yashiro et al.* [2004] shows that most of the slow CMEs ($u_0 < 250 \text{ km s}^{-1}$) are accelerated while most of the fast CMEs ($u_0 > 900 \text{ km s}^{-1}$) are decelerated within the combined field of view of the LASCO C2 and C3 telescopes [see also *Gopalswamy et al.*, 2001b, Figure 6].

[6] In order to see whether such a linear relationship holds near the Sun between the acceleration and speed of CMEs, we examined limb events in the SOHO/LASCO CME Catalogue (http://cdaw.gsfc.nasa.gov/CME_list/). We used only limb events to avoid projection effects. In favorable cases, we calculated u_c as an estimate of the ambient solar wind speed and compared them with in situ observations of solar wind speed by ACE/SWEPAM at 1 AU.

2. Method of Analysis

2.1. Data Source

[7] The SOHO/LASCO CME Catalogue [*Yashiro et al.*, 2004] lists CMEs detected by the LASCO Coronagraphs C2 and C3, which cover a combined field of view of 2.1 to 32 solar radii [*Brueckner et al.*, 1995]. For each CME, the heliocentric distance of the leading edge was measured at a position angle where the leading edge moved fastest. By fitting the height-time plot to first- and second-order polynomials, average speeds and accelerations of the CMEs are

obtained, respectively [*Yashiro et al.*, 2004]. In this paper we use the linear-fit speed as the initial speed u_0 and the curve-fit acceleration as the initial acceleration a_0 . The present analysis is based on the catalogue last updated on 22 April 2005.

[8] The solar wind data (http://www.srl.caltech.edu/ACE/ASC/level2/lvl2DATA_SWEPAM.html) used in this analysis were obtained by ACE/SWEPAM [*McComas et al.*, 1998], which measures the solar wind plasma electron and ion fluxes as functions of direction and energy.

2.2. Selection of CMEs

[9] For the purposes of this study, we use limb CMEs for which more than five height measurements were made because the estimation of acceleration is sensitive to the number of height measurements. The CMEs referred to as “halo” or “partial halo” are excluded from the present analysis to minimize projection effects.

[10] We start with low-latitude CMEs that appeared within 20 degrees from the equator. These are CMEs with position angle in the range of 90 ± 20 degrees (east limb) and 270 ± 20 degrees (west limb). CMEs that appeared at high or middle latitudes will be discussed later in section 3.4.

[11] For the available CMEs during the period from 1998 to 2003, the critical speeds u_c together with the linear coefficients c_1 are obtained statistically by sliding a 14-day window. It means that the estimated solar wind speed is a measure of the average speed for the 14-day period and does not reflect every-day variation. Results from a narrower window will be presented in section 3.3.

2.3. Chi-Square Fitting

[12] The critical speed u_c and the slope c_1 of equation (4) are obtained so that they minimize the quantity

$$S = \sum_{i=1}^{i=N} \frac{\{a_{0i} - c_1(u_{0i} - u_c)\}^2}{\sigma_{ai}^2 + c_1^2 \sigma_{ui}^2}, \quad (5)$$

where the subscript i denotes the i th CME, N is the number of CMEs in the 14-day period, and σ_{ai} and σ_{ui} are the measurement errors in a_{0i} and u_{0i} , respectively. Since the initial acceleration a_{0i} and the initial speed u_{0i} are obtained by fitting polynomial functions to the time-height plot of the leading edge of each CME, they are subject to errors arising from the fitting and errors arising from the measurement. The error in height measurement depends on the clarity of the CME feature tracked. On the assumption that both the

errors are random and independent, errors in a_{0i} and u_{0i} are obtained as

$$\sigma_{ai}^2 = \sigma_{ai1}^2 + \sigma_{ai2}^2$$

and

$$\sigma_{ui}^2 = \sigma_{ui1}^2 + \sigma_{ui2}^2,$$

where σ_{ai1} and σ_{ui1} are errors that depend on the clarity of the feature, while σ_{ai2} and σ_{ui2} are those arising from fitting.

[13] If the errors are normally distributed, the sum of squares of N random variables $a_{0i} - c_1(u_{0i} - u_c)$, each normalized by its variance $\sigma_{ai}^2 + c_1^2\sigma_{ui}^2$, is χ^2 -distributed [e.g., *Press et al.*, 1992]. (Here we assume that the errors in a_{0i} and u_{0i} are not correlated; however, it is not confirmed since we know σ_{ai}^2 and σ_{ui}^2 but not σ_{ai} or σ_{ui} . It should be noted that it might affect the results.) Once we have adjusted the two parameters c_1 and u_c so that they minimize the quantity S , the minimum S_{\min} is χ^2 -distributed for $N-2$ degrees of freedom. The hypothesis that the acceleration a_0 is modeled by equation (4) is rejected if the probability that S lies in an improbable “critical region” by chance is smaller than the level of significance α

$$\int_S^\infty f(\chi^2) d\chi^2 < \alpha, \quad (6)$$

where f is the probability density of the χ^2 distribution. In this analysis, we set the level of significance $\alpha = 0.01$ according to *Press et al.* [1992]. That is, we reject the result of fitting if S_{\min} is larger than the χ^2 value for $N - 2$ degrees of freedom,

$$S_{\min} > \chi_{N-2}^2(0.01), \quad (7)$$

at the significance level $\alpha = 0.01$ defined by

$$\alpha \equiv \int_{\chi_{N-2}^2(\alpha)}^\infty f(\chi^2) d\chi^2. \quad (8)$$

[14] Figure 1a is an example of good fitting. It shows the initial acceleration versus the initial speeds of low-latitude CMES above the east limb (position angle of $90 \pm 20^\circ$) observed during the period from 6 August 1999 to 20 August 1999. There were five CMES during the period, represented by five crosses in Figure 1a. Lengths of the bars indicate the magnitude of the errors σ_{ui} (horizontal bars) and σ_{ai} (vertical bars).

[15] For this period, the linear relationship is clearly recognized, and the data points agree well with the best-fit line representing equation (4). The slope $c_1 = -0.052 \times 10^{-3} \text{ s}^{-1}$ and the critical speed $u_c = 473.9 \text{ km s}^{-1}$ of the best-fit line are searched in $u_c - c_1$ space so that they minimize S . Figure 1b shows the contour map of S in $u_c - c_1$ space. The cross at $(u_c, c_1) = (473.9, -0.052)$ indicate the position of the minimum S_{\min} , and the contours are for $S = S_{\min} + 2.3$, $S = S_{\min} + 4.61$, and $S = S_{\min} + 9.21$. The gray, outermost contour outlines the area $S < \chi_3^2(0.01)$. As the minimum $S_{\min} = 0.947$ is smaller than the value $\chi_3^2(0.01) = 11.35$, the estimation is not rejected, and we accept critical speed u_c as the estimation of the ambient solar wind speed near the Sun.

[16] Figure 1c shows another example of successful fitting for the 14-day period starting from 10 June 1999.

Since all CMES on the last 3 days of the 14-day period did not pass the criteria of the data selection, the date of the observation of the last applicable CME within the 14-period, 21 June, is indicated in the panel. The errors are large for some of the CMES, but $S_{\min} = 10.09$ is smaller than the chi-square value $\chi_7^2(0.01) = 18.48$, and the fitting of the data to the model equation (4) is not rejected.

[17] Figure 1e is an example of rejection of the model fitting. During the 14-day period starting from 4 April 1999, there were no applicable CMES on the last 3 days. Among eight CMES in Figure 1e, some CMES deviate from the regression line and the deviations are larger than the errors. The parameters $u_c = 404 \text{ km s}^{-1}$ and $c_1 = -0.047 \times 10^{-3} \text{ s}^{-1}$ might be obtained, but the resultant $S_{\min} = 33.10$ is larger than the chi-square value $\chi_6^2(0.01) = 16.81$ for 6 degrees of freedom, so we reject the values obtained. Figure 1f shows the contour map of S , in which the gray contour for $\chi_6^2(0.01)$ does not appear as it is smaller than the minimum value S_{\min} . It shows that the probability that the sum S_{\min} takes such a large value is less than 0.01 (1%), thus the hypothesis that “the distribution is modeled by equation (4)” is rejected.

[18] Figure 1g shows an example for which no linear relationship is found. During the 14-day period starting from 22 September 1999, there were only four low-latitude CMES on the east limb within the first 5 days of the period. No relationship was found between the initial speed and acceleration. The slope c_1 is positive and almost vanishing. There are many other periods during which no linear relationship could be found. For such cases, it is useless to calculate the critical speed u_c , and we have to give up the estimation of solar wind speed.

2.4. Standard Errors in Estimated Speeds

[19] The standard errors in the parameters u_c and c_1 are respective projections onto the u_c and c_1 axes of the boundary of “the confidence region” that contains certain percentage of the total probability distribution [*Press et al.*, 1992]. In this study, we set the confidence level $\alpha = 0.01$, so there must be a 99% chance that the true parameter values fall within the confidence region around the measured value. The limiting contour value S_L for significance α is expressed as

$$S_L = S_{\min} + \chi_p^2(\alpha), \quad (9)$$

where $p = 2$ is the number of fitting parameters [*Lampton et al.*, 1976]. Table 2 reproduces the values of $\chi_p^2(\alpha)$ for $p = 2$. The black contours in Figures 1b and 1d correspond to $S_L = S_{\min} + \chi_2^2(0.32)$, $S_L = S_{\min} + \chi_2^2(0.10)$, and $S_L = S_{\min} + \chi_2^2(0.01)$. The last contour encloses the “the confidence region” of 99% confidence level. The projection onto the u_c axis gives the confidence limits of u_c , for example, $336 \text{ km s}^{-1} < u_c < 615 \text{ km s}^{-1}$ for Figure 1b.

3. Solar Wind Speed Estimated From Limb CMES

3.1. Results for East and West Limbs

[20] Figure 2a shows the critical speed u_c estimated from the CMES observed above the east limb for 14-day periods in 1999. The blanks for which no u_c was available are

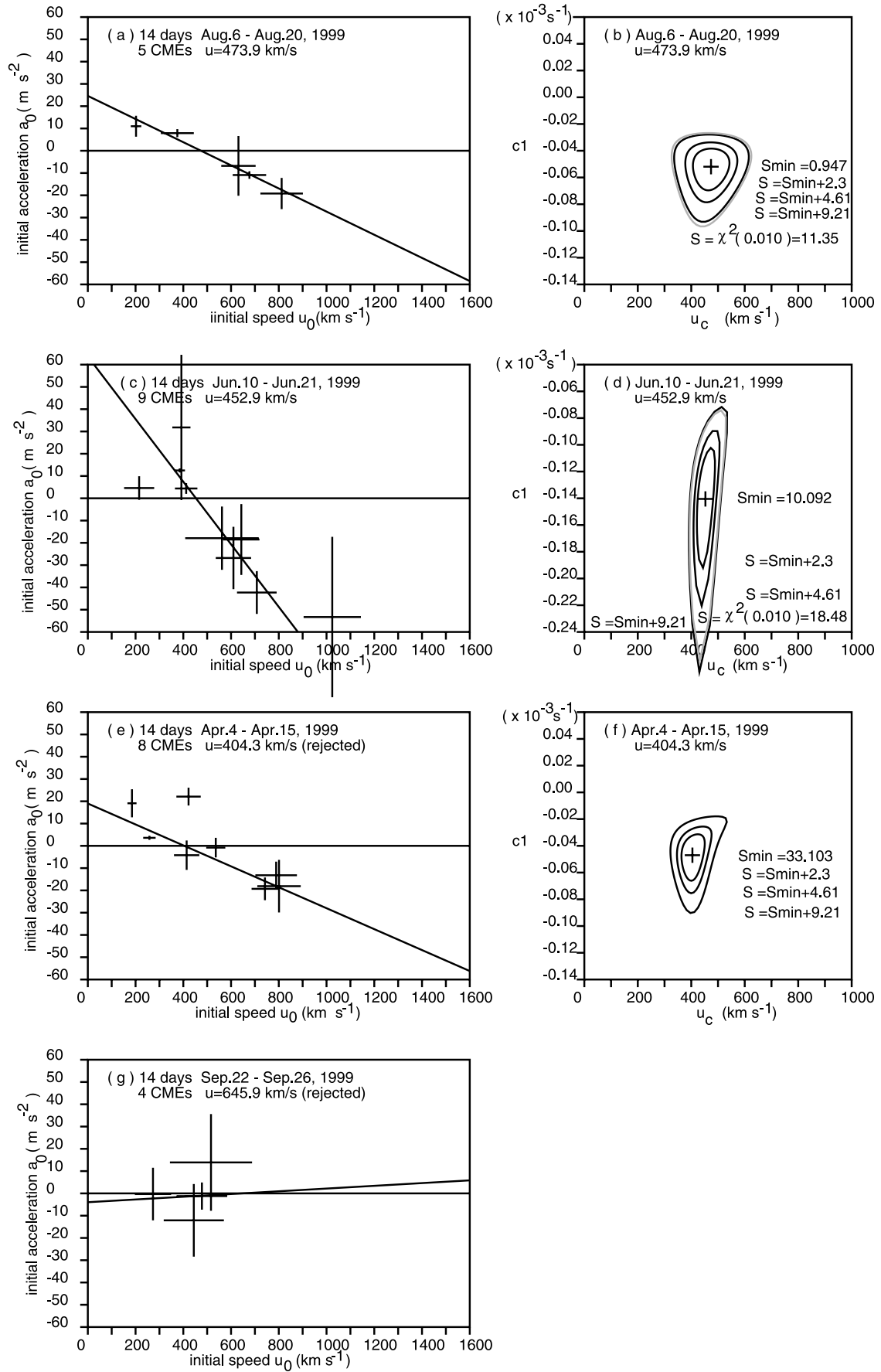


Figure 1

Table 2. Values of the Term $\chi^2(\alpha)$ for 2 Degrees of Freedom (Adapted From Table 1 of *Lampton et al.* [1976])

Significance α	Confidence	χ^2
0.32	0.68 (1 σ)	2.3
0.10	0.90 (1.6 σ)	4.61
0.01	0.99 (2.6 σ)	9.21

mainly due to the insufficient number of events or the large deviation of the data as expressed in equation (7). The standard errors in u_c are indicated by the vertical bars. There is 99% chance that the true value falls within the range. The speed u_c varied from 41 km s⁻¹ up to 571 km s⁻¹, within the range similar to but somewhat slower than the average solar wind speed detected near the Earth. In some cases, the standard errors are larger than 100%.

[21] Figure 2b shows the critical speed u_c estimated from the west-limb CMES. The speed u_c , within the range between 27 km s⁻¹ and 840 km s⁻¹, varies differently from those estimated from the east-limb CMES. For example, the estimated speed peaks around the days from 210 to 220 in Figure 2a, with values of u_c larger than 470 km s⁻¹, while it was flat in Figure 2b and u_c was lower than 270 km s⁻¹ during the same period. It is natural, as the estimations are for different solar sources.

[22] The results from the east and the west limbs are compared with each other in Figure 2c, after being shifted by $\pm 1/4$ rotation of the Sun (6.75 days), respectively. Since there is a time difference of 1/2 solar rotation between them, the solar source of the wind might evolve during the interval. Consistent estimates can be expected only in steady regions. Although some discrepancies are observed at around the days 105 and 250 in Figure 2c, the speeds estimated at the two limbs are often in good accordance with each other. For example, the estimation $u_c = 332\text{--}438$ km s⁻¹ in Figure 2b for the days 160–170, after being shifted, come into the transition from the fast wind $u_c = 537$ km s⁻¹ to the slower wind $u_c = 282$ km s⁻¹ estimated from the east limb CMES as recognized in Figure 2c at around the day 155. The slow winds $u_c < 270$ km s⁻¹ for the days 210–220 in Figure 2b fill in the blank in Figure 2a at the days 190–200 bounded by the slow speeds of $u_c < 290$ km s⁻¹ and $u_c < 150$ km s⁻¹. Thus the critical speed u_c can be an indicator of the speed of the solar wind in the vicinity of the Sun.

[23] The ambient solar wind speed thus obtained is compared with in situ measurement in interplanetary space. The solar wind speed $V_{1\text{AU}}$ measured by the SWEPAM instrument on board ACE at around 1 AU from the Sun is superimposed on Figure 2c. Since the solar activity or the magnetic configuration of the solar source of the wind may

evolve within the 1/4 rotation of the Sun and the solar wind speed itself may evolve in interplanetary space, we do not expect the solar wind speed measured at 1 AU to agree with the speed estimated from the limb CMES. Surprisingly, there are periods during which the near-Sun estimates agreed with the 1-AU measurements. For example, the estimate for days 140–180 in Figure 2c traces the variation of the solar wind speed observed by ACE, and the local peaks of u_c at around day 230 in Figure 2c reproduces the wind speed profile obtained by ACE. On the other hand, the estimated speeds are significantly lower than the measurements at 1 AU for days 200–220 in Figure 2c.

3.2. Comparison With in Situ Observations at 1 AU

[24] Figure 3 shows the critical speed u_c estimated from the limb CMES, together with the daily averages of the solar wind speed $V_{1\text{AU}}$ measured by ACE at 1 AU for each calendar year from 1998 to 2003. The dates of u_c estimates on each limb are shifted by $\pm 1/4$ solar rotation so that they correspond to the dates on which the source region faced Earth and ACE. The ACE data are shifted by the travel time 1 AU/ $V_{1\text{AU}}$ to their launch dates. The second panel is the same as that in Figure 2c.

[25] Although the “ambient” speeds estimated from limb CMES deviate from the ACE measurements mostly toward lower values, they sometimes agree with the 1-AU speed. For example, such an agreement is recognized for days 180 and 240 in 1999, for day 230 in 2000, and for days 100–110 in 2002. The agreement implies that sometimes the low-latitude solar wind completes acceleration within 20 R_S from the Sun. During other times there is additional acceleration beyond 20 R_S , as the 1-AU solar wind speed is greater than the solar wind speeds estimated in the vicinity of the Sun.

[26] Figure 4 shows histograms of the solar wind speed u_c estimated from the limb CMES together with those of the solar wind speed $V_{1\text{AU}}$ measured by ACE at 1 AU. The near-Sun solar wind speed ranges from 100 km s⁻¹ to 700 km s⁻¹, with 90% of them within the range; 90% of the 1-AU solar wind speeds ranged from 300 km s⁻¹ to 700 km s⁻¹. The upper limit is similar in both cases; the distribution of the estimated near-Sun wind speeds extends to lower speeds. This indicates that additional acceleration is acting on the solar wind plasma beyond a distance of 20 R_S from the Sun.

3.3. Reducing the Length of the Correlation Periods

[27] Since the solar wind speed depends on the location of the source on the Sun, one might think that selecting a shorter window would improve the spatial resolution of the

Figure 1. (a) The initial acceleration a_0 versus the initial speeds u_0 of five coronal mass ejections (CMEs) above the east limb detected in the latitude range $\pm 20^\circ$ from the equator observed during the period 4–20 August 1999. Lengths of the bars indicate the magnitude of the errors σ_{ui} (horizontal bars) and σ_{ai} (vertical bars). (b) The contour map of S for the period presented in Figure 1a. The central cross marks the position of the minimum S_{\min} . The gray contour is for $S = \chi^2(0.01)$ for $N-2$ degrees of freedom, and the black contours are for $S = S_{\min} + 2.3$, $S = S_{\min} + 4.61$, and $S = S_{\min} + 9.21$. The outermost black contour, projected onto the u_c axis, gives the confidence limit of u_c . (c) The linear fitting of nine CMEs observed during the period 10–21 June 1999. (d) The contour map of S for the period presented in Figure 1c. (e) The linear fitting of 8 CMEs observed during 4–15 April 1999. Some CMEs deviate largely from the regression line with $u_c = 404$ km s⁻¹ and $c_1 = -0.047$. The fitting is rejected because $S_{\min} = 33.10$ is larger than the chi-square value $\chi^2_6(0.01) = 16.81$ for 6 degrees of freedom. (f) The contour map of S for the period presented in Figure 1e. (g) The distribution of the CMEs for the period 22–26 September 1999. No relationship was found between the initial speed and the initial acceleration.

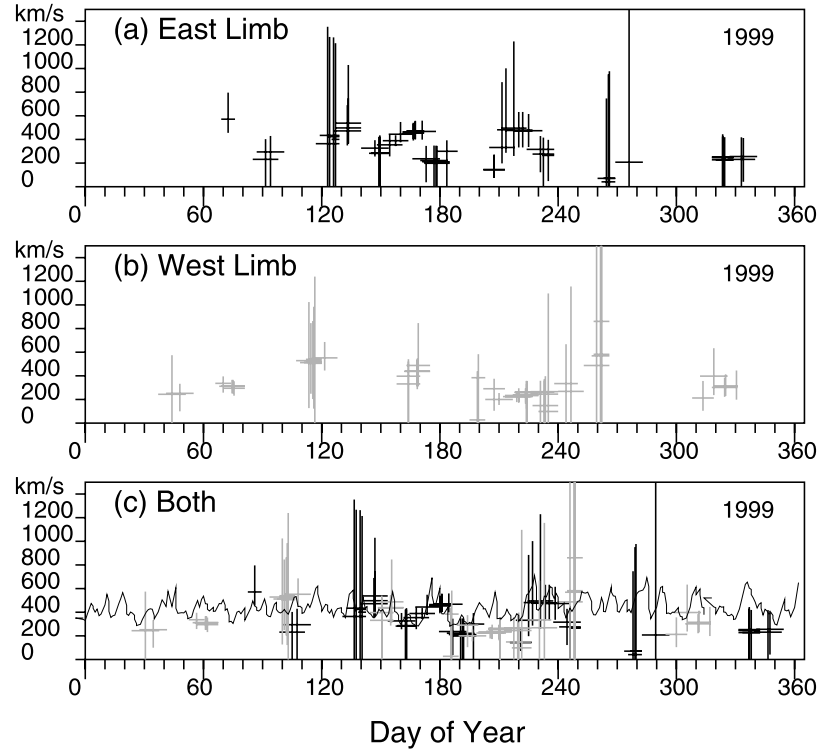


Figure 2. The solar wind speed u_c estimated from the low-latitude CMEs above (a) east and (b) west limbs. Each horizontal bar ends on the date of the last CME within the 14-day period. The standard error of each estimation is indicated by the vertical bars. (c) The speeds estimated above the east and the west limbs are compared with each other after being shifted by 6.75 days (1/4 rotation of the Sun). The 1-AU solar wind speeds ($V_{1\text{AU}}$) measured by ACE/SWEPAM are superimposed.

estimation of the solar wind speed. An attempt was made to shorten the 14-day window of the analysis to improve the temporal resolution. Figure 5a shows an example of the linear fitting for the 7-day period starting from 4 April 1999. Compared with the overlapping period presented in Figure 1e, the goodness-of-fit is improved by the selection of the narrower window. Figure 5b shows the contour map of S . $S_{\min} = 2.34$ is smaller than $\chi^2_{N-2}(0.01) = 13.28$ at the significance level $\alpha = 0.01$. The speed $u_c = 477 \text{ km s}^{-1}$ thus obtained agreed with the interplanetary measurement at 1 AU, as marked with an arrow in Figure 5c. On the other hand, setting the window shorter than 14 days reduces number of data points and thus reducing available intervals for solar wind speed estimate near the Sun. For example, the estimation for the days 340–350 of 1999 in Figure 3 is absent in Figure 5c.

3.4. Latitude Dependence of the Solar Wind Near the Sun

[28] In order to see whether we can detect possible dependence on latitude, the CMEs that appeared at higher latitudes are used in estimation of the “ambient” solar wind speed near the Sun. Figure 6 shows histograms of the solar wind speeds u_c estimated from high-, middle-, or low-latitude CMEs. The latitude of each CME is determined from the position angle at which height measurement was made. The distribution of u_c are systematically shifted to higher speeds at higher latitudes, although u_c are distributed over a wide range in each panel.

[29] Figure 7a shows the map of the solar wind speed in 1999 inferred from IPS technique [Kojima and Kakinuma, 1990]. The latitudinal structure is not very clear in 1999. On the other hand, as recognized in Figure 7b, the latitudinal structure is clearer in 1998. So possible latitude dependence was searched in the year, but no estimation of the speed u_c was available at higher latitudes in 1998 because of insufficient number of events.

4. Discussion

4.1. Summary of Estimation

[30] The critical speed u_c of equation (4) was calculated from the linear fitting of the initial accelerations a_0 and the initial speeds u_0 for CMEs detected on the east and west limbs of the Sun within 20 degrees from the equator for 14-day periods, on the expectation that it is an indication of the ambient solar wind speed close to the Sun. The value u_c , obtained with a 99% confidence level, sometimes agreed with the 1-AU solar wind speed, while in other cases it was smaller than the interplanetary measurements. The distribution of u_c ranged from 100 to 700 km s^{-1} . It is wider than the distribution of the solar wind speed measured at 1 AU, 300 to 700 km s^{-1} , and shifted to the lower values.

[31] The agreement between the estimated speed u_c and the solar wind speed measured at 1 AU suggests that at least in some periods the solar wind plasma is accelerated within 20 R_S up to the level of the wind speed at 1 AU. On the other hand, the smaller near-Sun speed than that at 1 AU suggests

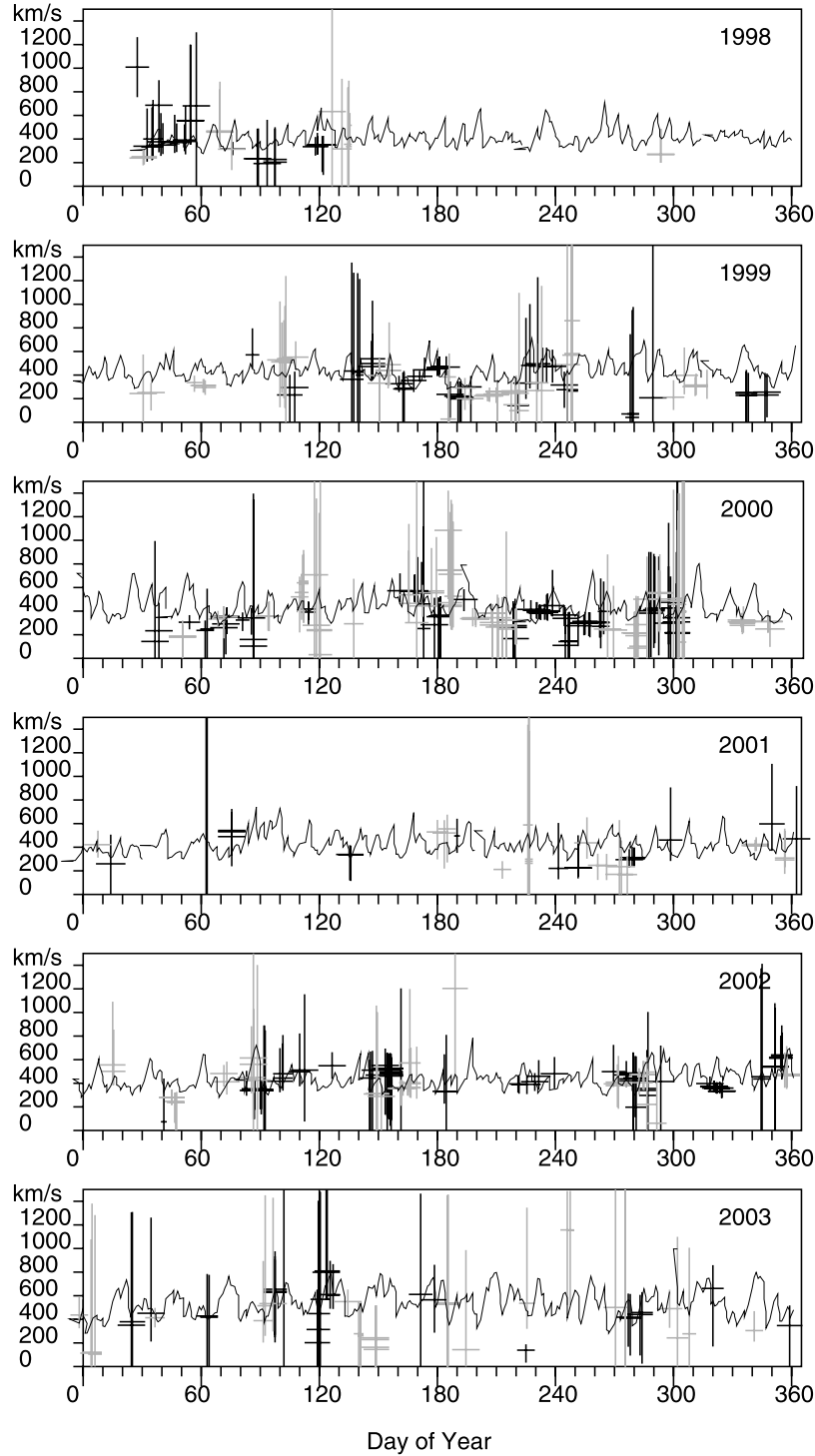


Figure 3. The ambient solar wind speed u_c (crosses) estimated from the low-latitude limb CMES, presented after being shifted for 1/4 solar rotation, and the 1-AU solar wind speed V_{1AU} measured by ACE/SWEPAM (curves). The ACE data are shifted by the travel time $1 \text{ AU}/V_{1AU}$ to their launch dates.

that sometimes the solar wind is subject to additional acceleration beyond $20 R_s$. Another possibility is that the discrepancies might be caused by the interplanetary detection of the CMEs because the estimation is for the “ambient” solar wind speed, while the spacecraft at 1 AU measures both the CMEs and the ambient solar wind.

4.2. Evolution of CME Speed

[32] Equation (2) describes the relationship between initial speed u_0 and average acceleration a , and equation (4) is for initial speed u_0 and initial acceleration a_0 . If the relationship holds throughout the interplanetary space as

$$a(t) = c_1(u(t) - u_c), \quad (10)$$

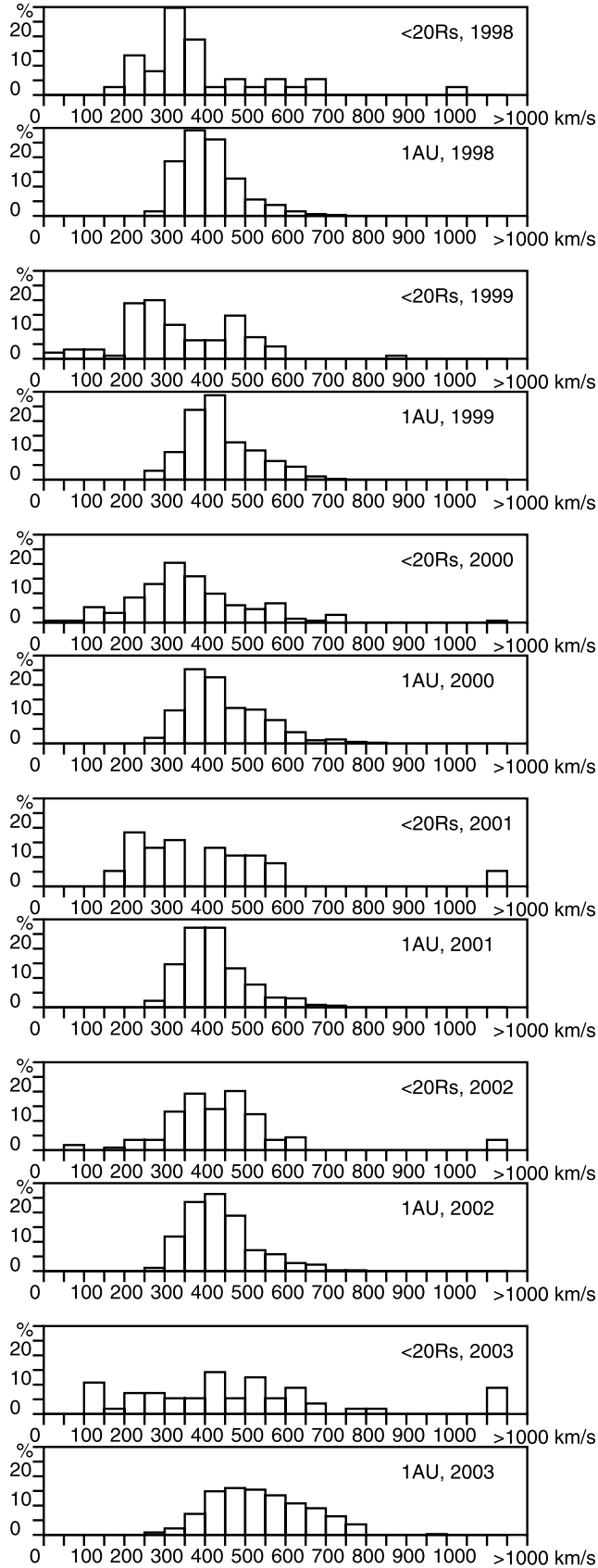


Figure 4. Histograms of the near-Sun ambient solar wind speed u_c estimated from the low-latitude limb CMES, and the 1-AU solar wind speed ($V_{1\text{AU}}$) measured by ACE/SWEPAM.

we can solve the differential equation to obtain the velocity

$$u(t) = u_c + (u_0 - u_c) \exp(c_1 t) \quad (11)$$

as a function of time t , together with the distance

$$r(t) = u_c t - \frac{u_0 - u_c}{c_1} \{1 - \exp(c_1 t)\} + 1R_S \quad (12)$$

[Nakagawa *et al.*, 2003].

[33] Figure 8 shows the evolution of the speeds $u(t)$ of CMEs which are released with a variety of initial speeds u_0 , plotted against the distance $r(t)$ from the Sun. Figure 8a is for $u_c = 406 \text{ km s}^{-1}$ and $c_1 = -0.54 \times 10^{-5} \text{ s}^{-1}$ determined from the average acceleration during the travel from the Sun to 1 AU [Gopalswamy *et al.*, 2001a], while Figure 8b is for $u_c = 474 \text{ km s}^{-1}$ and $c_1 = -0.52 \times 10^{-4} \text{ s}^{-1}$ determined from Figure 1a in this paper. In both cases the speed $u(t)$ converges to u_c , and the interplanetary speeds are less distributed than the initial speeds, but the convergence occurs too fast in Figure 8b, in which no variation remains in CME speeds in interplanetary space. It does not agree with the interplanetary observations.

[34] It suggests that the parameter c_1 obtained from the limb CMES within $20 R_S$ is too large to be used throughout the interplanetary space out to 1 AU. The values of c_1 determined from the limb CMES range from 10^{-5} to 10^{-4} s^{-1} , similar to the case of Figure 8b. Since the parameter c_1 is a measure of viscosity coefficient, it seems likely that c_1 is larger in the vicinity of the Sun than in interplanetary space far from the Sun.

4.3. Evolution of Ambient Solar Wind Speed

[35] In previous sections the critical speed u_c was handled as a constant; however, the ambient solar wind speed near the Sun is not constant but it increases with distance from the Sun. We have shown that in most cases the acceleration completes within $20 R_S$. Concerning the evolution of the ambient solar wind, Sheeley *et al.* [1997] analyzed moving coronal features that are thought to passively trace the solar wind outflow and obtained their speed at different heights. They employed a model function of the form

$$v(t)^2 = v_a^2 \left\{ 1 - \exp\left(-\frac{r(t) - r_1}{r_a}\right) \right\} \quad (13)$$

to fit the event observed by SOHO/LASCO on 30 April 1996. Here $v(t)$ is the solar wind speed, r_1 is the height of the first detection of the feature, and r_a is the scale height. The asymptotic speed v_a was 418 km s^{-1} . Differentiating this equation, we obtain

$$a(t) = \frac{v_a^2}{2r_a} \exp\left(-\frac{r(t) - r_1}{r_a}\right), \quad (14)$$

which shows that the acceleration occurs mainly within $r < r_a + r_1$, where $r_a = 15.2 R_S$ and $r_1 = 4.5 R_S$ for this event. This agrees with our result that the acceleration completes within $20 R_S$ in most cases. By substituting equation (13) into equation (14), we obtain

$$a(v) = -\frac{1}{2r_a} (v^2 - v_a^2), \quad (15)$$

which is a parabola in v - a space, in contrast to a straight line by equation (4). It is interesting to note that equation (15)

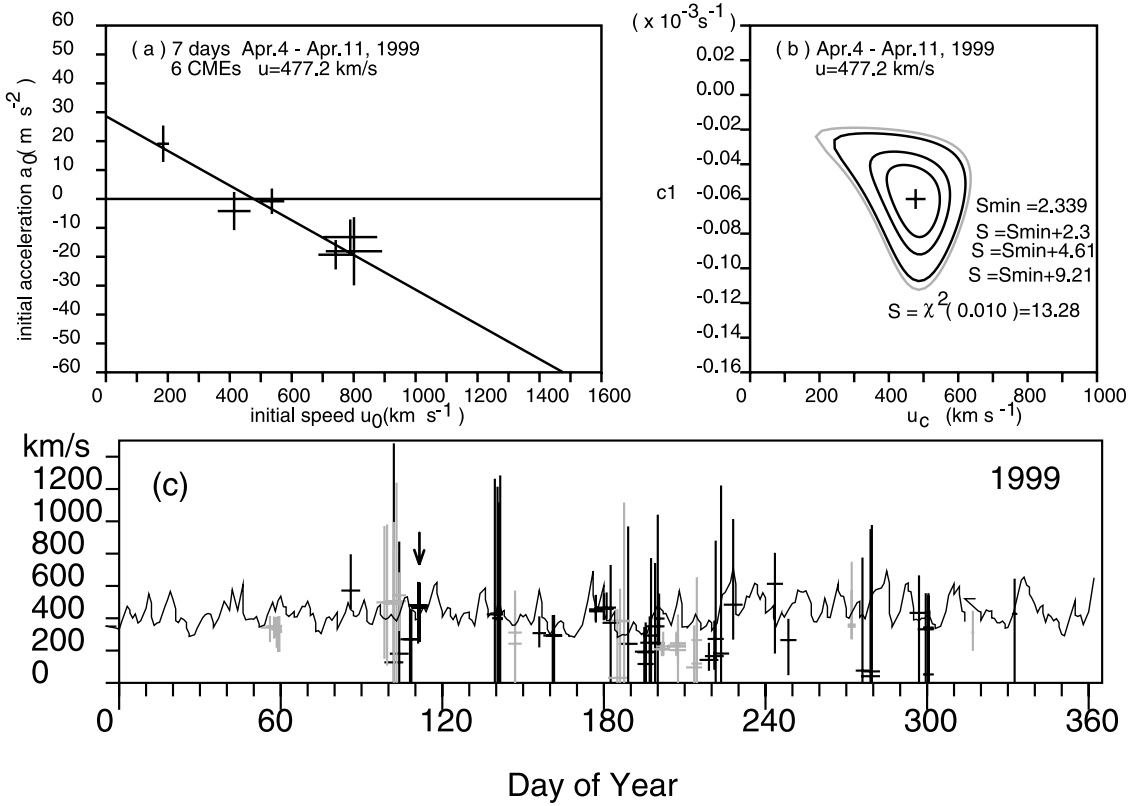


Figure 5. (a) The initial acceleration a_0 versus the initial speeds u_0 for six CMEs above the east limb observed during the 7-day period, 4–11 April 1999. (b) The contour map of S for the period presented in Figure 5a. (c) The ambient solar wind speed u_c estimated from the low-latitude limb CMEs for 7-day periods. The array indicates the estimation from the period presented in Figure 5a.

gives $a = 0$ at $v = v_a$, and the slope, $-\frac{v}{r_a}$ for equation (5), becomes $-0.39 \times 10^{-4} \text{ s}^{-1}$ at $v = v_a$, in good accordance with our c_1 value obtained from limb CMEs.

[36] It should be noted that u_c is an estimate over the height range $2.1\text{--}20 R_S$, not at $20 R_S$. When height measurements are limited to low altitude where the local solar wind speed v is smaller than the asymptotic value v_a , a CME with initial speed u_0 between v and v_a might decelerate in spite of u_0 being smaller than v_a in the very early stage of ejection. This may cause an underestimate of u_c .

[37] It is not easy to obtain low-altitude estimates of the solar wind speed by limiting the heights of CME measurements. In such low altitudes where the solar wind is still accelerating, there must be forces other than the drag, i.e., the propelling force which acts on all CMEs up to a few solar radii, and the gravity. Contributions a_p and $-a_g$ from the propelling force and gravity, respectively, should be added to the right-hand side of equation (4), giving $a = 0$ when all three forces balance. Use of equation (4) implicitly assumes that $a_p - a_g$ is negligible with respect to the drag, which is not applicable to CMEs near the Sun. In the present analysis, the contributions from the propelling force and gravity would be negligible over the coronagraph field of view.

5. Conclusion

[38] The solar wind speed in the vicinity of the Sun is estimated using the linear relationship between initial speed

and acceleration of coronal mass ejections that appeared on the limb of the Sun. The estimated speeds were close to but somewhat lower than the solar wind speed measured at 1 AU. The result suggests that sometimes the low-latitude solar wind completes accelerating within $20 R_S$ from the Sun, while the acceleration continues beyond $20 R_S$ during

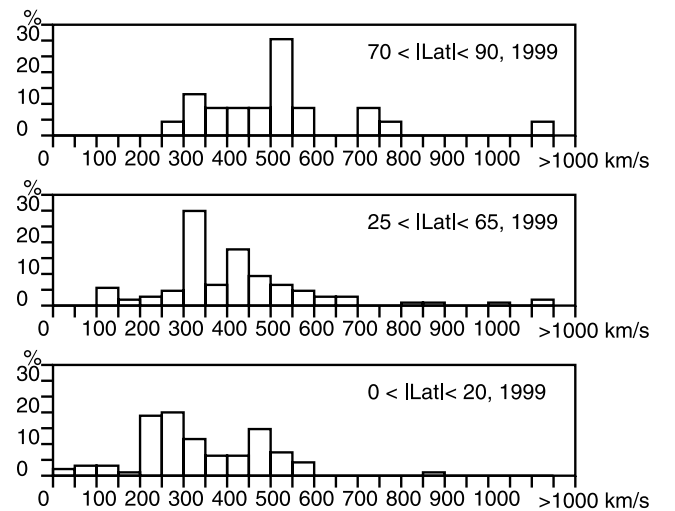


Figure 6. Histograms of the near-Sun ambient solar wind speed u_c in 1999 estimated from the high-latitude, middle-latitude, and low-latitude CMEs.

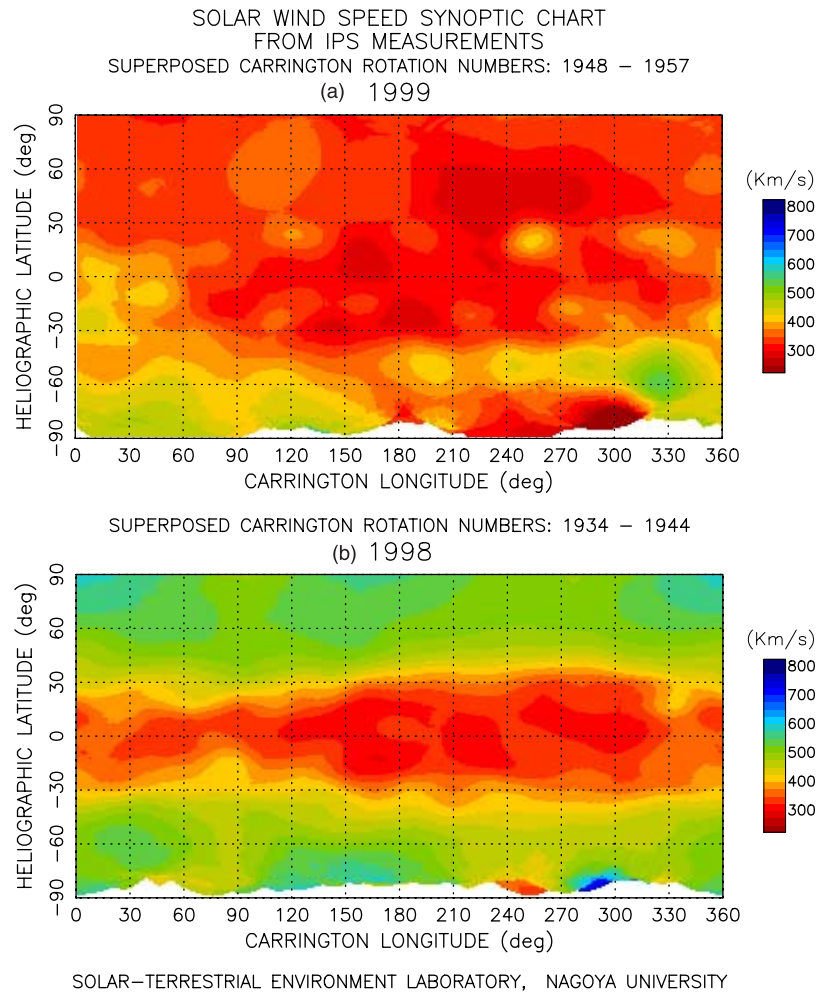


Figure 7. The solar wind velocity observed by using the technique of interplanetary scintillation in (a) 1999 and (b) 1998. By courtesy of STE Laboratory, Nagoya University (<ftp://stesun5.stelab.nagoya-u.ac.jp/pub/vmap/>).

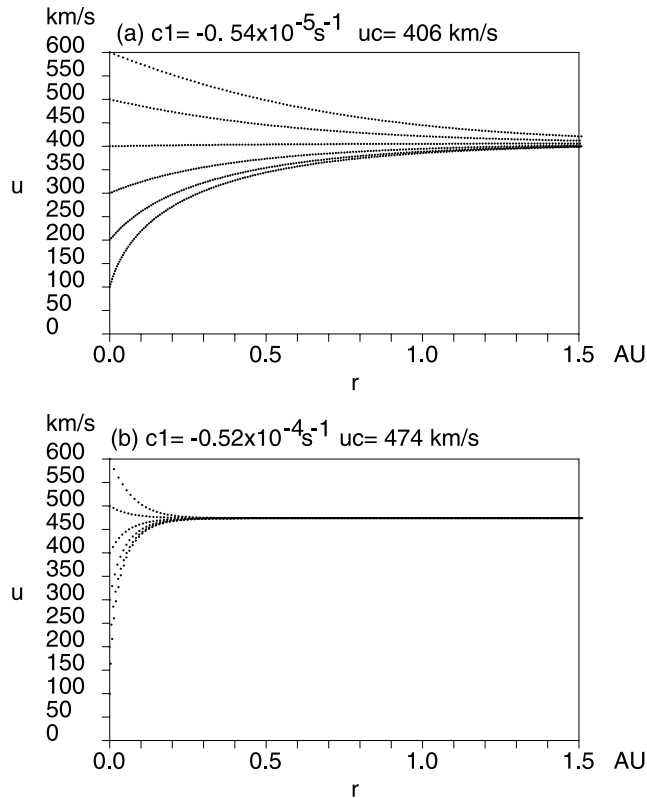


Figure 8. Evolution of CME speeds $u(t)$ with different initial speeds u_0 , as a function of the distance $r(t)$ from the Sun. (a) Calculation for $u_c = 406 \text{ km s}^{-1}$ and $c_1 = -0.54 \times 10^{-5} \text{ s}^{-1}$ determined from the average acceleration during the travel from the Sun to 1 AU [Gopalswamy et al., 2001]. (b) Calculation for $u_c = 474 \text{ km s}^{-1}$ and $c_1 = -0.52 \times 10^{-4} \text{ s}^{-1}$ determined from the linear relationship between u_0 and a_0 for the period 6–20 August 1999.

other times. The method presented here provides a simple means of estimating solar wind speed near the Sun. Currently, we have to use limb observations to get the speed by accounting for solar rotation. STEREO observations can provide data for immediate estimate.

[39] **Acknowledgments.** The SOHO/LASCO CME catalog is generated and maintained by NASA and the Catholic University of America in cooperation with the Naval Research Laboratory. SOHO is a project of international cooperation between ESA and NASA. The authors are indebted to David J. McComas for ACE/SWEPAM data. Velocity maps in Figure 7 are by courtesy of M. Tokumaru, STE Laboratory, Nagoya University. Interplanetary scintillation measurements of the solar wind were carried out under the joint research program of the Solar-Terrestrial

Environment Laboratory of Nagoya University. This work was partly supported by the JSPS grant-in-aid for scientific research project 17540424. [40] Shadia Rifai Habbal thanks William A Coles and Daniel Winterhalter for their assistance in evaluating this paper.

References

- Brueckner, G. E., et al. (1995), The Large Angle Spectroscopic Coronagraph (LASCO), *Solar Phys.*, **162**, 357–402.
- Burlaga, L. F., L. Klein, N. R. Sheeley Jr., D. J. Michels, R. A. Howard, M. J. Koomen, R. Schwenn, and H. Rosenbauer (1982), A magnetic cloud and a coronal mass ejection, *Geophys. Res. Lett.*, **9**, 1317–1320.
- Gosling, J. T., E. Hildner, R. M. MacQueen, R. M. Munro, A. I. Poland, and C. L. Ross (1975), Direct observations of a flare related coronal and solar wind disturbance, *Solar Phys.*, **40**, 439–448.
- Gopalswamy, N., A. Lara, R. P. Lepping, M. L. Kaiser, D. Berdichevsky, and O. C. St.Cyr (2000), Interplanetary acceleration of coronal mass ejections, *Geophys. Res. Lett.*, **27**, 145–148.
- Gopalswamy, N., A. Lara, S. Yashiro, M. L. Kaiser, and R. A. Howard (2001a), Predicting the 1-AU arrival times of coronal mass ejections, *J. Geophys. Res.*, **106**, 29,207–29,217.
- Gopalswamy, N., S. Yashiro, M. L. Kaiser, R. A. Howard, and J.-L. Bougeret (2001b), Characteristics of coronal mass ejections associated with long-wavelength type II radio Bursts, *J. Geophys. Res.*, **106**, 29,207–29,217.
- Kojima, M., and T. Kakinuma (1990), Solar cycle dependence of global distribution of solar wind speed, *Space Sci. Rev.*, **53**, 173–222.
- Lampton, M., B. Margon, and S. Bowyer (1976), Parameter estimation in X-ray astronomy, *Astrophys. J.*, **208**, 177–190.
- Lindsay, G. M., J. G. Luhmann, C. T. Russell, and J. T. Gosling (1999), Relationships between coronal mass ejection speeds from coronagraph images and interplanetary characteristics of associated interplanetary coronal mass ejections, *J. Geophys. Res.*, **104**, 12,515–12,523.
- McComas, D. J., S. J. Bame, P. Barker, W. C. Feldman, J. L. Phillips, P. Riley, and J. W. Griffee (1998), Solar wind electron proton alpha monitor (SWEPAM) for the Advanced Composition Explorer, *Space Sci. Rev.*, **86**, 563–612.
- Nakagawa, T., A. Matsuoka, and NOZOMI/MGF team (2003), NOZOMI observation of transient, non-spiral magnetic field in interplanetary space associated with limb CMES, in *Solar Wind Ten*, edited by M. Velli, R. Bruno, and F. Malara, *AIP Conf. Proc.*, **679**, 117–120.
- Press, W. H., S. A. Teukolsky, W. T. Vetterling, and B. P. Flannery (1992), *Numerical Recipes in C: The Art of Scientific Computing*, 2nd ed., Cambridge Univ. Press, New York.
- Richardson, I. G., C. J. Farrugia, and D. Winterhalter (1994), Solar activity and coronal mass ejections on the western hemisphere of the Sun in mid-August 1989: Association with interplanetary observations at the ICE and IMP8 spacecraft, *J. Geophys. Res.*, **99**, 2513–2529.
- Schwenn, R. (1983), Direct correlations between coronal transients and interplanetary disturbances, *Space Sci. Rev.*, **34**, 85–99.
- Sheeley, N. R., Jr., R. A. Howard, M. J. Koomen, D. J. Michels, R. Schwenn, K. H. Muhlhauser, and H. Rosenbauer (1985), Coronal mass ejections and interplanetary shocks, *J. Geophys. Res.*, **90**, 163–175.
- Sheeley, N. R., et al. (1997), Measurements of flow speeds in the corona between 2 and 30 Rsun, *Astrophys. J.*, **484**, 472–478.
- Yashiro, S., N. Gopalswamy, G. Michalek, O. C. St.Cyr, S. P. Plunkett, N. B. Rich, and R. A. Howard (2004), A catalogue of white light coronal mass ejections observed by the SOHO spacecraft, *J. Geophys. Res.*, **109**, A07105, doi:10.1029/2003JA010282.

N. Gopalswamy and S. Yashiro, NASA Goddard Space Flight Center, Code 695.0, Greenbelt, MD 20771-0001, USA.

T. Nakagawa, Information and Communication Engineering, Tohoku Institute of Technology, Taihaku-ku, Sendai, 982-8577 Miyagi, Japan. (nakagawa@tohtech.ac.jp)